Bonding Analyses of Unconventional Carbon Allotropes

Marc Esser,[a] Arina A. Esser,[b] Davide M. Proserpio,[b,c] and Richard Dronskowski[a,d,*]

[a]Institute of Inorganic Chemistry, RWTH Aachen University, Landoltweg 1, 52056 Aachen, Germany

[b]Samara Center for Theoretical Materials Science, Samara State University, Ac. Pavlov Street 1, Samara 443011, Russia

[c]Dipartimento di Chimica, Università degli Studi di Milano, Via Golgi 19, 20133 Milano, Italy

[d]Jülich-Aachen Research Alliance (JARA-FIT and JARA-HPC), RWTH Aachen University, 52056 Aachen, Germany

*Corresponding author. Tel: +49 241 80-93642. E-mail: drons@HAL9000.ac.rwth-aachen.de

Abstract

Utilizing first-principles electronic-structure calculations, we present the chemical-bonding analyses of hypothetical carbon allotropes based on tetrahedral structure motifs such as T-carbon, TY-carbon and T-graphene. While previous publications on these novel allotropes have dealt with *ab initio* phonon, band structure and DOS calculations, the focus of this work is the partitioning of the band-structure energy in terms of bonding, nonbonding and antibonding contributions. We re-evaluate the chance of making such allotropes by careful bond analyses and compare them to already known equivalents, namely diamond, graphene

*Corresponding author. Tel: +49 241 80-93642. E-mail: drons@HAL9000.ac.rwth-aachen.de

and the Buckminsterfullerene molecule. A synthetic route is proposed to a new compound, called TY-carbodiimide, that exhibits similar structure and bonding properties as TY-carbon.

1. Introduction

With the discovery of the buckminsterfullerene molecule by Kroto *et al.* [1] in 1985 mankind entered the era of carbon allotropes, only fifteen years after its first proposal by Osawa based on a discussion of bond angles and π-bonding energies [2]. For a long time, carbon is known to be one of, if not *the* most versatile element in the periodic table. Due to its ability to form C-C bonds of different character (often dubbed as "sp^3"-, "sp^2"- and "sp"-type bonds) the theoretical variety of carbon allotropes is sheer endless as illustrated with the Samara Carbon Allotrope Database (SACADA) [3]. This structural diversity comes with unique physical properties as suggested by the experience of diamond and graphite which were the only known carbon allotropes before the groundbreaking discovery of the C_{60} molecule [1]. The latter also opened the world of synthetic carbon allotropes. C_{60} and its derivatives are nowadays used as functional materials with many applications. In fact, no other compound class surpasses it as electron acceptor in solar cells [4].

The subsequent years brought forth the discovery of the carbon nanotube (1991) [5], the first organic metal with very high charge-carrier mobility. As the mechanically strongest material known to man, it is now used to reinforce synthetic composite materials. Graphene (2004) [6]—single layers of graphite—is currently discussed as a base for field-effect transistors, probably the only device with application of quantum-field theory [7].

Naturally, the interest in predicting and synthesizing new functional materials based solely on carbon is exceptional. Over the last five years, three promising structures based on inserting a tetrasymmetrical structure motif in already known allotropes were proposed: T-carbon [8], TY-carbon [9] and T-graphene [10]. We use the term "tetrasymmetry" in accordance with the established literature [10] and it denotes a symmetric relationship

between four aspects of an object: in case of a tetrahedral motif (T-carbon, TY-carbon) it is the four faces of the tetrahedron and in case of the tetra-rings of T-graphene it is the four vertices that constitute the tetra-ring (the structural details are discussed below). According to SACADA [3], their underlying topological nets are augmented diamond **dia-a** for the first two and 4.8^2-**fes** for the latter, using the three-letter designations introduced by M. O'Keeffe [11] Their (crystal) structures are displayed in Fig. 1.

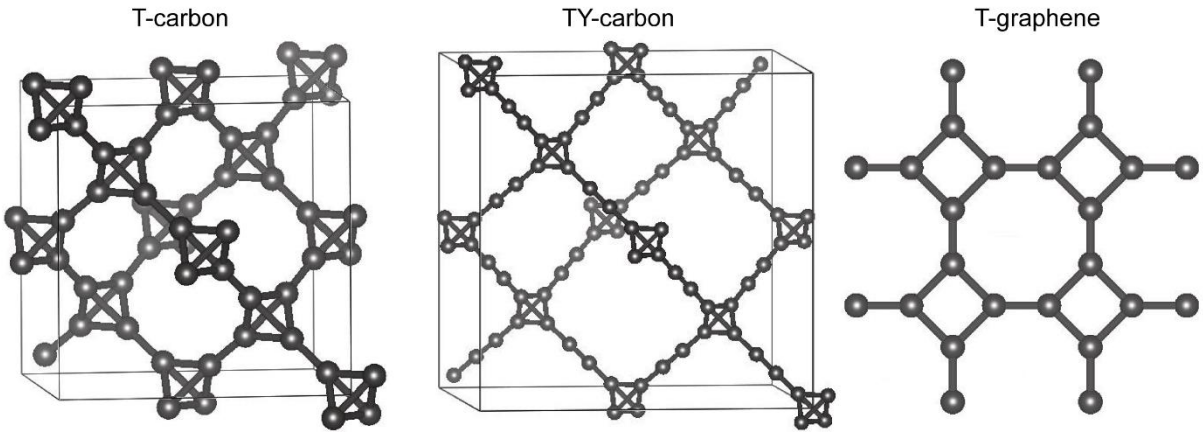

Figure 1: From left to right: the crystal structure of T-carbon, TY-carbon (**dia-a**) and T-graphene (4.8^2-**fes**).

T-carbon (Fig. 1, left) is essentially a diamond type but with each carbon atom replaced by a C tetrahedron (a geometrical operation called *augmentation*, hence the name **dia-a**). This approach is "rationalized" by the tendency of carbon to form sp^3 hybrids, four degenerate orbitals which are directed toward the corner of a tetrahedron, leading to very high stability. There is a fundamental difference, though, in how the tetrahedral structure motif is implemented: while diamond shows T_d symmetry around every atom, T-carbon shows T_d symmetry only around the empty *center* of each tetrahedron. The corner atoms forming said empty tetrahedra are also tetrahedrally coordinated by four other carbon atoms, just like in diamond. The elementary difference is that these tetrahedra are distorted and have only three

mirror planes instead of six, as mandatory for proper T_d symmetry. For reasons of simplicity we will nonetheless refer to the local structural motif as being tetrahedral throughout.

TY-carbon (Fig. 1, middle) is derived from T-carbon by implementing two C≡C triple bonded "spacer" atoms between the tetrahedral units. Finally, T-graphene (Fig. 1, right) is a tetrasymmetrical variation of the 2D allotrope graphene, formed by replacing the hexagonal honeycomb structure of graphene by a tiling made up of tetrarings (squares) and octagons, as proposed in one of the earliest works on hypothetical carbon allotropes by Balaban and collaborators in 1968 [12]. Recently, this allotrope re-surfaced in the literature and has been treated to first principles investigations for the first time [10] [13]. Once synthesized, a plethora of applications has been suggested in previous works for these new materials: For example, T-carbon could be used as a material comparable in hardness with diamond at a much lower density, or as a container for hydrogen storage, exploiting the cavernous structure [8]. The material's band gap was computed to 3 eV, indicating semiconducting behavior with possible electronic applications [8]. All of the mentioned possible utilizations hold true for TY-carbon as well, with the exception that it is even less dense and exhibits larger caverns to be filled with guest atoms [9]. TY-carbon has also been predicted to be a semiconductor but its band gap depends on the length of the triple bond. For the equilibrium bond length a small band gap of about 1.5 eV was calculated, comparable to silicon's 1.1 eV gap, making it even more interesting for the design of electronic devices [9]. While T-graphene shares a lot of properties with already known graphene, it might possess an extended portfolio of features, for instance, enhanced electron concentration at p–n junctions in semiconductor devices built from doped T-graphene [10].

Despite the importance of the total energy to judge a compound's stability compared to other polymorphs, it tells nothing about the underlying reasons which *cause* this energetic difference, *i.e.*, the bonding nature inside the solids. This vital information shall be unveiled within this work to gain further insight into the three promising candidates for the next

carbon-only functional materials. To do so, we utilize crystal orbital Hamilton population (COHP) [14] analysis to dissect the band-structure energy into orbital-pair interactions and their bonding contributions, as well as a newly developed visualization tool for levels which are constituted by sp^3-orbital mixing, dubbed mixing DOS (MDOS) [15]. A detailed report about the utilized theoretical tool box constitutes the upcoming section.

2. Theoretical Methodology

To assess the stability – and thus the possibility of a future synthesis – of these materials, density-functional theory (DFT) calculations were performed. We used the generalized-gradient approximation (GGA) by Perdew, Burke, and Enzerhof [16], employing the projector-augmented wave (PAW) method [17] as implemented in VASP [18] [19] [20], revision 5.3.5. The utilized potential employs the common $2s^2 2p^2$ valence configuration, with the $1s^2$ electrons treated as being core-like. We chose to not go to higher-level approaches beyond GGA-PBE (e.g., utilizing dispersion corrections) to ensure comparability of our results with the previous publications [8] [9] [10].

A plane-wave cutoff of 500 eV was used as the convergence criterion. The Brillouin zone was sampled utilizing **Γ**-centered **k**-point meshes according to the Monkhorst-Pack scheme [21]. For T-carbon, a mesh density of $7 \times 7 \times 7$ was used. For all other bulk materials, the number of **k**-points in each dimension was adjusted according to the reciprocal vectors to yield comparable **k**-point densities. For TY-carbon and TY-carbodiimide this equates to a mesh of $3 \times 3 \times 3$ points. In the case of T-graphene, vacuum slabs of 10 Å were employed to eliminate interaction between adjacent layers and a reduced cell with two tetra-rings was used. The **k**-mesh was fixed to $15 \times 7 \times 3$ points for this cell. The crystal structures were taken from the literature [8] [9] [10] and fully optimized until self-consistency in the total energy was reached within 10^{-6} eV/cell. The bond length, lattice parameter and total energy values of the novel carbon allotropes could all be reproduced to the accuracy given in the literature [8] [9] [10]. In case of the less exotic allotropes, reduced hexagonal cells with

two atoms (diamond, graphene) and four atoms (graphite) were simulated. To reach a **k**-mesh density for these small cells consistent with the T-allotropes, a grid of 27 × 27 × 27 points was employed for diamond and a mesh of 23 × 23 × 7 points was used for graphite and graphene. For C_{60}, a cubic cell with 30 Å edge length was created, in which the molecule was placed in such a way that the distance to its translational images exceeds 23 Å. For this cell, the Brillouin zone was sampled at the **Γ**-point exclusively. To obtain the phonon density of states, such calculations were conducted utilizing the PHONOPY software package which harnesses the finite-displacement methodology [22]. While the TY-carbodiimide unit cell can readily be used for phonon calculations, as it boasts large cell parameters exceeding 15 Å, a 2 × 2 × 2 supercell (cell parameters exceeding 13 Å) was created for SiC_2N_4 to ensure force attenuation inside the cell. **Q**-meshes of 8 × 8 × 8 points were applied in both cases.

All DOS and COHP information was extracted from PAW functions by analytical projection onto a minimal local basis set of Slater-type atomic orbitals as implemented into the computer program LOBSTER (local-orbital basis suite towards electronic-structure reconstruction) [23] [24] [25]. After projection, LOBSTER reconstructs the entire PAW function via the LCAO (linear combination of atomic orbitals) technique. This projection scheme has been crucial for bond analyses for many advanced materials and problems that have been previously inaccessible to quantum-chemical investigation, *e.g.*, the local bonding nature in amorphous phase-change materials [26], chemical bonding at surfaces [27] [28] and spin-gapless graphitic carbon nitride semiconductors [29].

An in-house modified version of LOBSTER was employed to yield a previously introduced quantity dubbed MDOS, which serves as a visual indicator for orbital mixing (or "hybridization"), specifically "sp^3" mixing at this point in time [15]. This technique has recently been generalized to fit the orientation of the local basis to the local structural motifs in any given solid [30]. Thus, for the first time an analysis of the interplay of the canonic orbitals forming mixed levels can be achieved for the proposed allotropes.

3. Results and Discussion

As a starting ground of our discussion of the proposed tetrasymmetrical carbon allotropes, we recapitulate in Tab. 1 the total energies of these structures and how they compare to known carbon allotropes.

Table1: Total Energies of various hypothetical and existing carbon polymorphs (listed from lowest to highest in energy, relative to graphite (middle column) and in absolute values (right column)).

Structures	**Δ*E* (kJ/mol)**	***E* (eV/atom)**
Graphite	0	–9.218
Graphene	0.2	–9.216
Diamond	12.4	–9.090
C_{60}	35.8	–8.847
T-graphene	49.1	–8.709
TY-carbon	114.2	–8.034
T-carbon	125.6	–7.916

Of all carbon modifications, graphite displays the lowest total energy, just followed by graphene, another form constituted of solely a single layer of graphite. The energy difference is 0.2 kJ/mol—minute when compared to the energetic difference between graphite and diamond of 12.4 kJ/mol. And yet, thanks to a kinetic barrier, diamond is not only metastable at standard conditions but also the hardest substance known. Moving on to C_{60}, we have an allotrope even higher in energy (35.8 kJ/mol compared to graphite) which is stable enough for large-scale industrial production; indeed, metastable phases can possess enough structural integrity to be useful. With that being said, let us move on to the three novel suggested

polymorphs. T-graphene is 13.3 kJ/mol up the energy ladder than C_{60}, a small difference compared to the gap of 23.4 kJ/mol between C_{60} and diamond. TY-carbon, in contrast, displays the largest total energy-gap compared to its energetically closest cousin T-graphene of 65.1 kJ/mol. Finally, T-carbon is with its 125.6 kJ/mol relative to graphite, 11.4 kJ/mol higher in total energy than TY-carbon. We note in passing that interpenetrating versions of T- and TY-carbon, called T-II-carbon and TY-II-carbon, were suggested as novel high-pressure phases by Li *et al*. [31]. They are constructed by shifting the original cell by ½ the lattice vector along *a* and stacking original and copy together to produce a denser version of the original cavernous structures (see supplementary information for crystal structures and bonding analyses). The stacking in T-II-carbon leads to long-range interaction between the interpenetrating structures that feature prominent antibonding interactions from 0–16 eV on the energy scale. Accordingly, T-II-carbon is less stable than T-carbon (ΔE = 150.3 kJ/mol relative to graphite). The interpenetrating parts of TY-II-carbon are about 4.8 Å away from each other, so there is no significant bonding interaction. Hence TY-II-carbon does not significantly deviate from TY-carbon (ΔE = 114.1 kJ/mol). Because the interpenetrating structures show no improved stability over the originally proposed forms at zero pressure, we will not consider them any longer. Before moving on, we like to mention that the results of Li *et al*. show that T-II-carbon becomes energetically more favorable than T-carbon at pressures above 6.8 GPa, so T-II-carbon can be considered a novel high-pressure phase [31]. Since the authors found imaginary frequencies at zero pressures for TY-carbon, no further pressure-related simulations were performed.

We emphasize that meta-stability is no disqualifier for a potential synthesis or industrial application of a phase. Thus, it is vital to note that the kinetic stability of the three hypothetical allotropes has been shown before via phonon calculations, but shall not be part of our discussion here as this has been already thoroughly covered [8] [9] [10]. Instead, we direct our attention to the underlying reasons of the energetic differences, *i.e.*, the chemical bonding.

Figure 2 shows the local structural motifs (top) of the diamond-derived tetrasymmetrical allotropes alongside diamond itself. The structures are accompanied by the atom-projected local DOS (LDOS, middle), which we will re-examine in an *l*-resolved way (*l* being the azimuthal quantum number signifying the orbital nature, *e.g.*, s, p, d, f and so forth) as a starting ground for our investigation of the local bonding nature. The bottom part displays the MDOS of each structure, with which we will continue our scrutiny (more details in the upcoming paragraph).

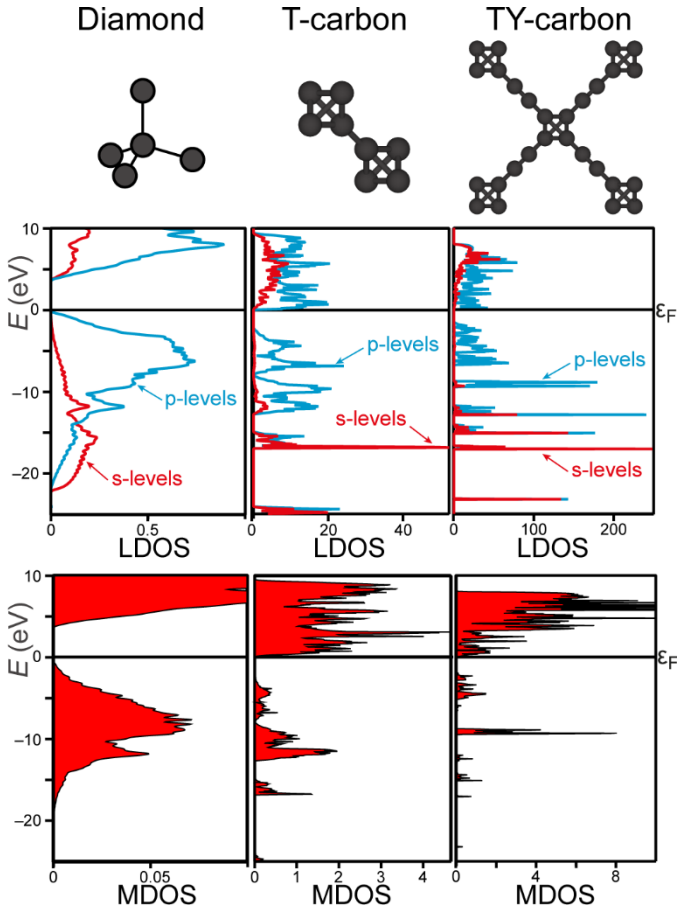

Figure 2: From left to right: local structural motif (top), local DOS (middle) and MDOS for sp^3-mixed levels (bottom) of diamond, T-carbon and TY-carbon.

Diamond's perfect tetrahedral angle of 109.5° produces s- and p-levels that overlap well on the energy scale (Fig. 2 top and middle left), an evidence of strong s-p orbital mixing. The

center part of Figure 2 shows the structural motif and DOS of T-carbon. Even though T-carbon is also built from tetrahedral units, the tetrahedral angle has a value of just 60°. This leads to s- and p-levels that are mostly separated on the energy scale, an indicator for less orbital mixing. The cavernous nature manifests itself in the electronic structure as molecule-like flat bands with low band dispersion, resulting in non-overlapping peaks in the DOS, because the tetrahedral units are electronically rather isolated compared to the tetrahedra in diamond with its well dispersed bands. Similar observations hold true for TY-carbon (Fig. 2, top and middle right).

To further investigate whether less hybridization/orbital mixing is found in T- and TY-carbon, a recently presented technique for detecting the effective amount of sp^3-*orbital mixing* is employed [15]. For this, a heuristic indicator was constructed on the basis of Pauling's findings regarding the ideal coefficient values to form the best bonding sp^3-functions. Nonetheless, we do not introduce any such unitary basis set-transformation, but stay with canonical atomic orbitals and analyze how close the effective mixing coefficients come to Pauling's ideal values. The indicator adopts values between zero and unity, unity indicating perfect sp^3-mixed levels and zero indicating no mixing at all. This measure then weights the DOS to produce the so-called mixing DOS (MDOS), as to be seen at the bottom of Fig. 2 for diamond, T-carbon and TY-carbon.

Immediately the reader will notice the broad appearance of sp^3-mixed levels in diamond, (Fig. 2, bottom left), that span virtually the entire energy range from –20 eV up to the Fermi edge—a direct result from energetically overlapping s- and p-levels seen before. T-carbon with its smaller overlap between s-and p-levels evidences (Fig. 2, bottom center) as having considerable less mixed levels compared to diamond, as expected. Even less sp^3-mixing can be noted for TY-carbon (Fig. 2, bottom right). To quantify these qualitative results, we use a previously introduced [15] technique of simply calculating the percentage of electron density situated in mixed levels via formula (1):

$$\mathrm{sp^3\ mixing\ (\%)} = \frac{\int_{-\infty}^{\varepsilon_F} \mathrm{MDOS}(E)dE}{\int_{-\infty}^{\varepsilon_F} \mathrm{DOS}(E)dE} \cdot 100 \qquad (1)$$

Hence, there is 5.8% of effective sp^3-mixing for diamond, 3.6% for T-carbon and 1.5% for TY-carbon, all in perfect accordance with the qualitative results extracted from the DOS of Fig. 2 with the naked eye alone.

Moving on to T-graphene, its DOS is shown together with the local structural motif on the right side of Fig. 3 accompanied by its parent allotrope graphene (Fig. 3 left).

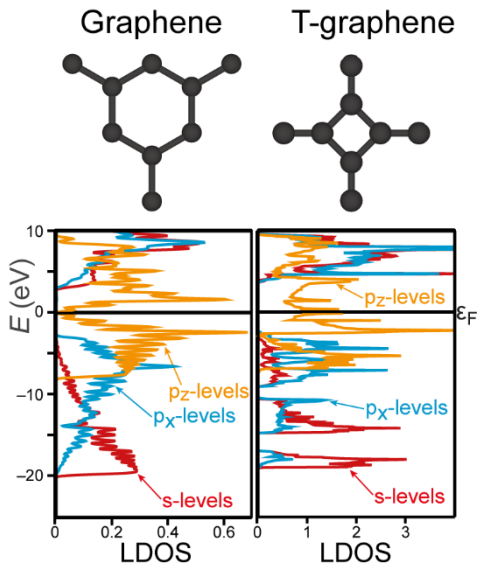

Figure 3: The same as Fig. 2 but for graphene and T-graphene. The LDOS of the p_x- and p_y-levels is identical for these allotropes, thus we do not show the p_y-levels for reasons of clarity.

Graphene and T-graphene show lots of similarities in their DOS: for both allotropes, the s-, p_x- and p_y-levels are well mixed and strong sp^2-hybridization is to be expected. The p_z-levels generate the graphite-familiar π-system located above and underneath the structural skeleton and is energetically situated in the DOS around ε_F. In sharp contrast to graphene (Fig. 3 left), however, the π-system of T-graphene (Fig. 3 right) does not vanish at the Fermi edge but displays occupied states which turn T-graphene into a metallic conductor.

To assign bonding properties to the DOS, projected COHPs (pCOHP) for the individual symmetry-inequivalent bonds were calculated. Before we will examine the results for the novel allotropes, we will recall the utility of the pCOHP tool by looking at the parent structures diamond and graphene first, accompanied by buckminsterfullerene, the latter chosen as a prime example for a cavernous, yet stable, all-carbon material to which T-carbon and TY-carbon can be compared.

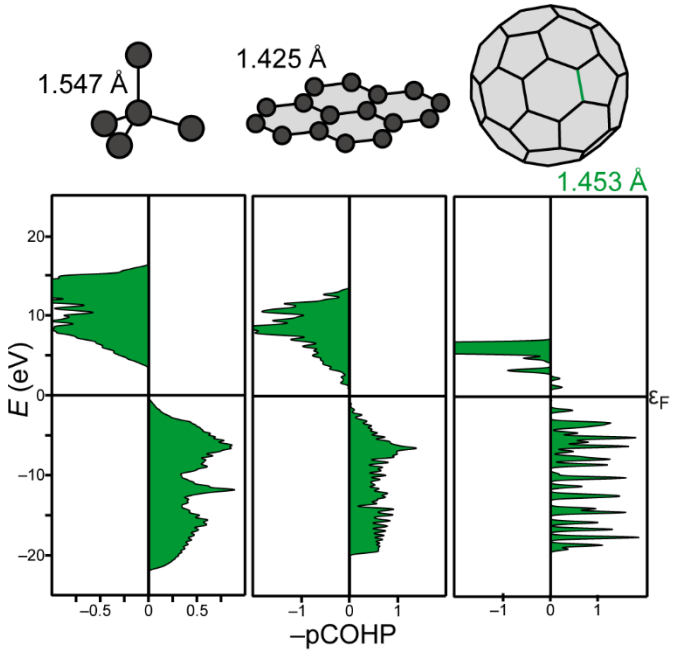

Figure 4: Projected COHPs of three important carbon allotropes, from left to right: diamond, graphene, buckminsterfullererene. Like all experimentally available carbon forms, they exhibit no antibonding levels below ε_F. To let bonding levels got to the right, –pCOHPs have been plotted, as usual.

The pCOHP uses the Hamiltonian matrix elements between two atoms to effectively weight the DOS by the bond energy. In principle, negative values (energy lowering) are produced for bonding interaction, positive ones for antibonding and zero for non-bonding interaction. Hence, bonding interactions go to the right and antibonding interactions to the left. By looking at the allotropes in Fig. 4, the reader notices at a glance that all three experimentally available allotropes evidence only filled bonding levels. For sake of

simplicity, we just show one of the two symmetry-inequivalent bonds of C_{60}, since both are similar in terms of their bonding attributes.

Now, let us examine the bonding of the three proposed allotropes, starting with T-carbon. In the top part of Fig. 5 the bonding nature within a tetrahedral unit and between these building blocks is analyzed.

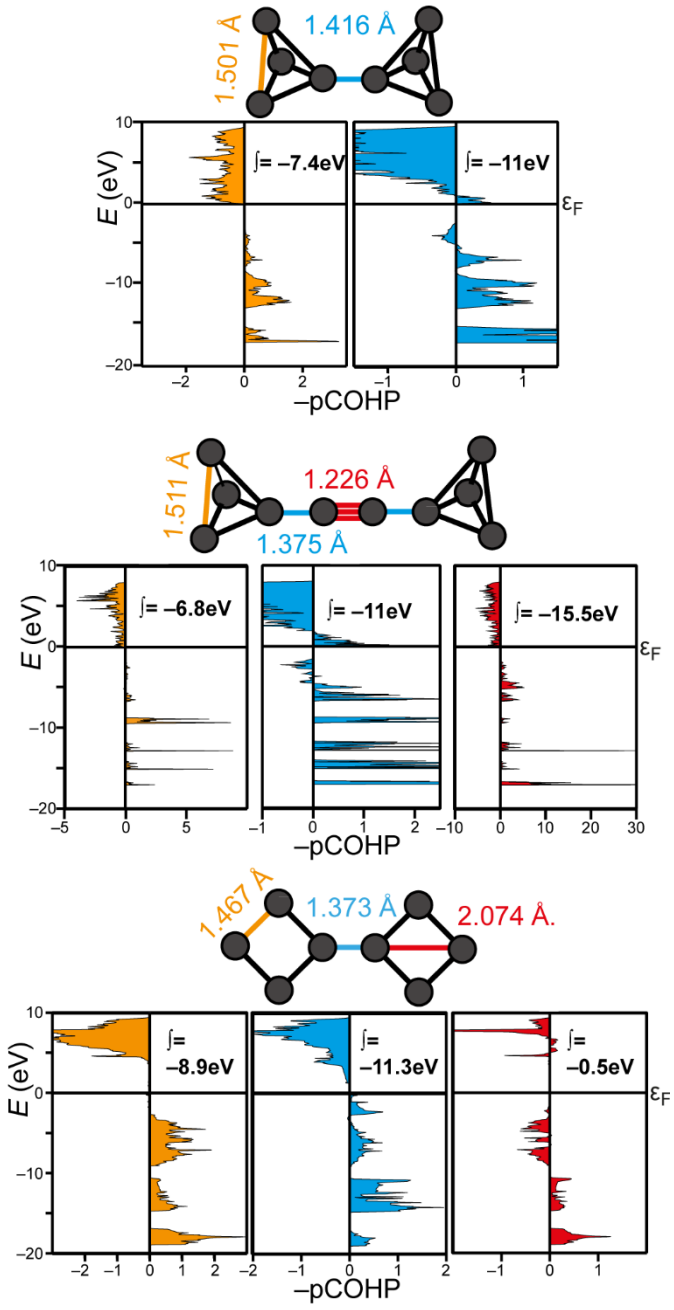

Figure 5: Projected COHPs for the symmetry inequivalent bonds in T-carbon, TY-carbon and T-graphene. All three proposed allotropes show filled antibonding levels, a phenomenon never before seen in carbon-only structures.

The inter-tetrahedral bond length is 1.416 Å, considerably shorter than the intra-tetrahedral bonds with 1.501 Å. The pCOHP integrals reveal that the bond-length-bond-strength rule holds true because the shorter bond between the T-units is 49 % stronger than the larger one. In addition, the inter-tetrahedron bond exhibits a very unusual property: while the main bonding peak (–15 to –17 eV) has largely s-character (as evident from the DOS, Fig. 2 center), the higher p-bands do not contribute much stabilization—in contrast, there is even a filled antibonding area from –2 to –5 eV, which cannot be seen in other carbon allotropes[†].

TY-carbon differs from T-carbon only by the presence of two "spacer" atoms inserted between the tetrahedral units. This similarity leads to the presence of antibonding levels in the same energy window between –2 and –5 eV (Fig. 5 middle), as found in T-carbon. While the intra-tetrahedral bond is about as long as before (Δd = 0.01 Å), there is a significant drop in bond strength, as evident from the difference in the ICOHP values of 0.6 eV, somewhat unexpectedly. The connecting bond from the tetrahedron to the triple bonded atom exhibits antibonding levels in the same energy range as the inter-tetrahedral bond in T-carbon. Consistent with the appearance of the antibonding fingerprint is the same ICOHP value for both bonds of –11 eV, even though the TY-carbon's bond is by 0.041 Å shorter. The stability of TY-carbon is mainly created through the inserted triple bond, which is the strongest (ICOHP = –15.5 eV) and also shortest bond (1.226 Å) in the allotrope.

The results indicate that electron density is being "pushed" from the tetrahedron into the interconnecting bonds: the farther away from the tetrahedron, the more advantageous for the system as the lower total energy of TY-carbon (–8.034 eV/atom) in comparison to T-carbon (–7.916 eV/atom) suggests. This is due to a strain within the tetrahedron: the bonding angle

[†] To validate this result, calculations with the TB-LMTO-ASA program were performed, which also exhibit this antibonding fingerprint region (results are not shown here).

has a value of 60° compared to 109.5° in diamond. For comparison, diamond was calculated to have a total energy of –9.090 eV/atom (see also Tab. 1).

Moving on from the diamond-like allotropes to T-graphene (Fig. 5 bottom), we note that the tetrasymmetrical square ring structure motif produces bonding angles of 90°. This is considerably smaller than the ideal of 120° for sp^2-hybridization, which explains the rise in energy of 48.9 kJ/mol compared to graphene. Here, again we can find the unusual fingerprint of antibonding states, as seen before, but now extending from –2 eV all the way down to –10 eV. In contrast to T- and TY-carbon, this fingerprint does not occur in the bonds linking the individual tetra-units, but within the tetraring itself. While both, the bonds either creating the ring structure, 1.467 Å, or the intra-connecting bond, 1.373 Å, show exclusively filled bonding levels, a wider contact across the ring was found, which carries the characteristic antibonding signature of the tetrasymmetrical carbon allotropes. In contrast to T- and TY-carbon, this bond is of not much importance for the stability of the structure, as it is by far the longest (2.074 Å) and weakest bond, as evident from the ICOHP (–0.5 eV). As in T-carbon, the stability of the allotrope is largely created by the interconnecting bonds between the tetra-units.

So far we can note a strong correlation between bond angles stemming from tetra-symmetry and the appearance of the antibonding pattern discovered. To further investigate this finding, a series of calculations isolating two tetrahedra from the relaxed T-carbon structure were performed, varying the tetrahedral bonding angle from 60° to 109.5°. We stress that this is not to be confused with a transformation pathway from T-carbon to diamond because, due to the different nature of tetrahedra in both structures (as discussed before), an angle change *cannot* transform one structure into the other. We focus here on the empty tetrahedra of T-carbon and the influence of the tetrahedral angle on the interconnecting bond. The isolated tetrahedra were valence saturated with hydrogen, hence a ditetrahedrane molecule.

For each geometry shown in the top of Fig. 6, the pCOHP of the interconnecting bond between both tetrahedra was calculated, as well as the local DOS (LDOS in short) of the two involved atoms. Naturally, the pCOHP and DOS of the isolated clusters show the typical molecule-like spikes stemming from a low amount of band dispersion. At the 60° angle, the pCOHP displays the antibonding fingerprint near the Fermi edge (highlighted in red in the second row of Fig. 6), just as found in T-carbon. The associated DOS show that these antibonding regions are created solely by p-orbital interactions. In the energetic region of the main bonding peak at ca. –12 eV, the DOS indicates some weak s- and p-orbital interaction. Upon increase of the tetrahedral angle to 79.8°, the antibonding fingerprint region significantly diminishes. In the according DOS, a shift of a s-peak situated at ca. –5 eV to –3 eV can be detected, as it is moving closer to the p-levels that generate the antibonding peak below the Fermi edge. Upon increasing the tetrahedral angle to 99.6° this s-peak is moving further up the energy scale, closing the gap between s- and p-levels. The overlap of s- and p-orbitals transforms the bonding nature just below the Fermi edge from antibonding to bonding. Further angle increase to 109.5° leads to a perfect overlap of s- and p-levels below the Fermi edge, resulting in a more pronounced bonding peak. The results reinforce that, also in the solid state, the antibonding fingerprint stems from a strain inside the tetrahedral units, leading to an energetic separation of s- and p-levels close to the Fermi edge in the interconnecting bonds. Those non-mixed p-levels are then responsible for generating the antibonding fingerprints that were found to be characteristic for the tetrahedral symmetry in carbon crystals.

It is straightforward to expect a pronounced increase of sp^3-mixed levels in the MDOS in the fingerprint region when going from 60° bonding angle to 109.5°. Indeed, there are no sp^3-mixed levels in the MDOS in the fingerprint energy window (Fig. 6 bottom, first entry) for a bonding angle of 60°. Upon angle increase to 79.8° a slight peak arises in the fingerprint region (highlighted with an exclamation mark) which gets increasingly more pronounced as

the angle is approaching the perfect tetrahedral angle of 109.5°, reaching finally its maximum just as the s- and p-peaks display perfect overlap in the DOS (Fig. 6 bottom, last entry), as discussed before. Also, applying formula (1) to the series of geometries yields an overall rise of electron density in sp^3-mixed levels, starting at 0.63 % and going all the way up to 1.34 %.

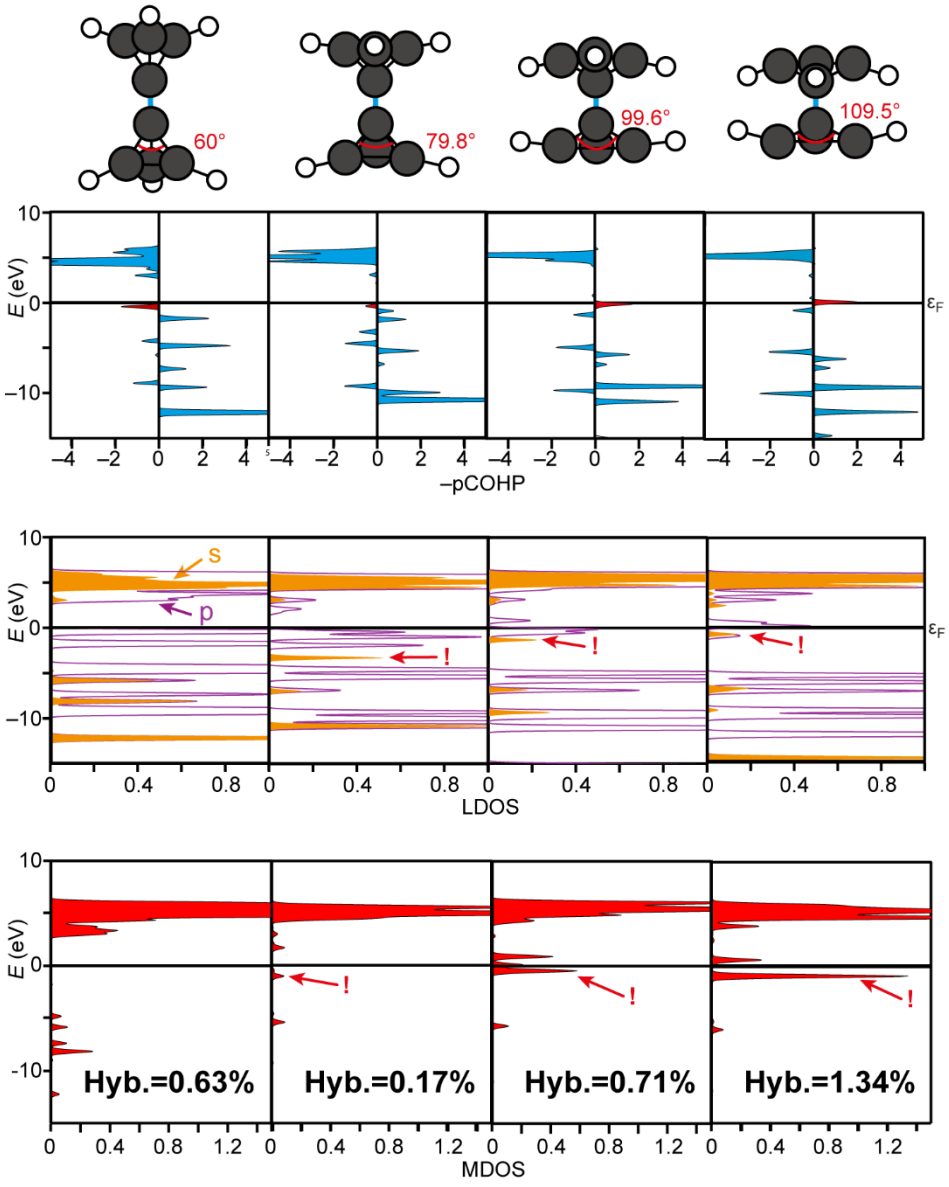

Figure 6: Structural sketch (first row) illustrating the geometry change in ditetrahedrane upon tetrahedral angle variation. COHPs (second row) computed for the interconnecting bond between the two tetrahedral units highlighted in blue in the geometry displayed in the top row of this figure. The third row shows the local DOS of the atoms forming the bond specified before. The s-levels are shown in filled orange curves; the p-states are shown in purple. MDOS of sp^3-mixed levels in the bottom row.

We want to complete our discussion with a possible synthetic route to the TY-structure, but, other than before, not as a pure carbon compound but modified with carbodiimide units. We dubbed this compound TY-carbodiimide, accordingly. While the interesting property portfolio was discussed in the original publications concerning the T-allotropes, no synthetic route was suggested concerning T- and TY-carbon and just a physical way was proposed to obtain T-graphene via epitaxial growth of carbon on metal layers, *e.g.*, a nickel (111) surface. While this might work for a sheet of T-graphene, there is no physical nor chemical way known at this time that could yield, even in theory, the cavernous structures of the diamond-based T-allotropes. The introduction of another element in TY-carbon—essentially replacing the two "spacer" atoms that separate the tetrahedra by carbodiimide units—opens up the possibility to obtain the TY-structure by a chemical *reaction*. At the same time, we preserve the unique topology of the structure and thus the unique bonding situation, as will be discussed in a short moment. Our compound, dubbed TY-carbodiimide, shares its chemical composition C_3N_2 with polymorphs predicted to be superhard semiconductors by Tian *et al.* in 2008 [32]. Despite the same composition, these polymorphs are radically different from our carbodiimide in terms of structure and properties: they are derived from simple cubic C_{20}, in which certain carbon atoms are replaced by nitrogen. Hence, these compounds do not belong to the class of carbodiimides and are not comprised of the specific tetrahedral structure motif of T- and TY-carbon.

We propose a synthesis based on fully chlorinated isolated tetrahedral units, C_4Cl_4, and

cyanamide, H_2NCN. The chlorinated tetrahedra can be obtained from already available tetra-*tert*-butyltetrahedrane [33] as synthesized in 1978 by Maier *et al.*. The chemical equation reads:

$$C_4Cl_4 + 2\,H_2NCN + 4\,\mathrm{Pyr} \rightarrow \underbrace{2\,C_3N_2}_{\mathrm{TY-carbodiimide}} + 4\,\mathrm{Pyr}\cdot\mathrm{HCl} \qquad (2)$$

with pyridine (Pyr) added in stoichiometric amounts to separate the sideproduct HCl. Now, the chemical reaction will take care of inserting the "spacer" units between the tetrahedra, while the resulting topology of TY-carbodiimide is already predetermined by the use of the single tetrahedra as educt. Cyanamide has been known to participate in similar kinds of reactions for a long time, for instance [34]:

$$2\ R_3SiCl + H_2NCN + Pyr \rightarrow\ R_3Si{-}NCN{-}SiR_3 +\ Pyr \cdot HCl. \quad (3)$$

Alternatively, similar syntheses using derivatives of H_2NCN may be tried, as has been shown before in other reactions [34] [35] [36]:

$$MnCl_2 + ZnNCN \rightarrow\ MnNCN +\ ZnCl_2 \quad (4)$$

and

$$2\ CrCl_3 + 3\ ZnNCN \rightarrow\ Cr_2(NCN)_3 +\ 3\ ZnCl_2 \quad (5)$$

and

$$2\ R_3SiCl + Ag_2NCN \rightarrow\ R_3Si{-}NCN{-}SiR_3 +\ 2\ AgCl \quad (6)$$

The reaction energy was gauged via the total energies to be 102 kJ/mol. Despite the predicted endergonic nature, the formation of HCl can aid as a driving force towards the right side of formula (2), as this byproduct can be withdrawn from the system—a common technique to facilitate energetically intricate reactions.

The structure of TY-carbodiimide bears striking resemblance to the phase SiC_2N_4 synthesized in 1997 by Riedel *et al.* [37]. It consists of Si atoms which are tetrahedrally coordinated by NCN-units (Fig. 7, top left). In fact, SiC_2N_4 was synthesized in a quite similar way resembling our formula (2) [37]:

$$n\ MeRSiCl_2 + 2\ H_2NCN\ + 2n\ Pyr \rightarrow [{-}\ MeRSi{-}\ NCN{-}\ ]_n\ +\ 2n\ Pyr \cdot HCl \quad (7)$$

$$n\ SiCl_4 + 2n\ Me_3Si{-}NCN{-}SiMe_3 \xrightarrow{Pyr,T=100°C} [SiC_2N_4]_n\ +\ 4n\ Me_3SiCl \quad (8)$$

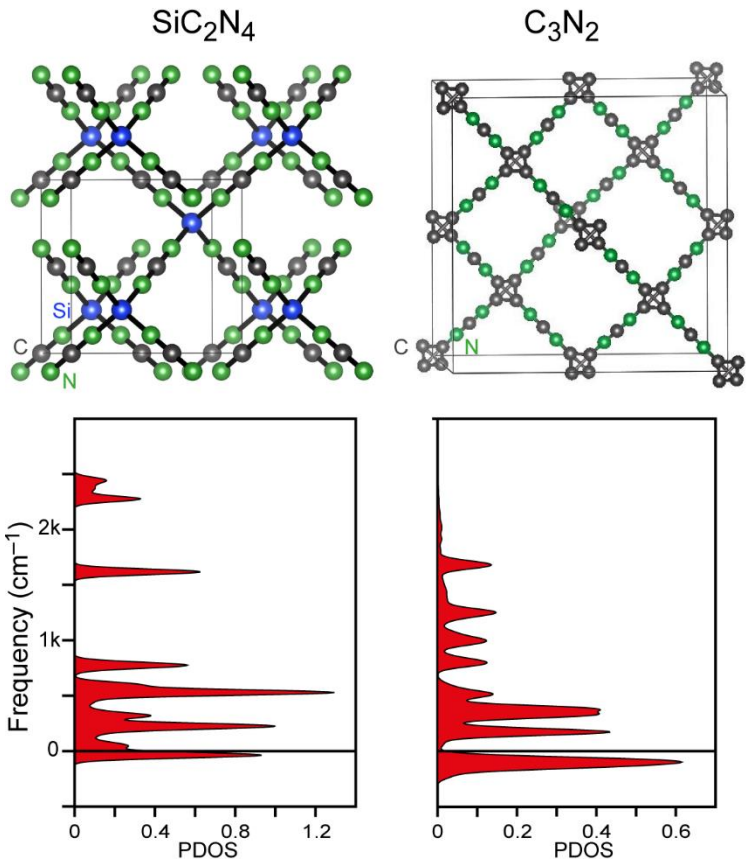

Figure 7: Crystal structure and phonon-DOS of synthetically available SiC_2N_4 (left side) and the predicted TY-carbodiimide C_3N_2 (right side), a proposed modified version of TY-carbon.

The phonon-DOS (PDOS) of SiC_2N_4 shows occupied imaginary modes (Fig. 7, left bottom) which stem from vibrations that have the NCN-units swing out of the connecting vector between the Si atoms—yet, the phase can be experimentally obtained in large yields. The NCN vibrations lead to a measurable macroscopic effect, namely a strongly negative thermal expansion as observed by Kroll *et al.* [38]. The higher the temperature, the higher the amplitude of these vibrations, which in turn forces the silicon atoms to come closer together. The reason of these oscillations to appear in our calculations particularly in the imaginary range is due to the nature of the experimental structure model as obtained by Riedel *et al.*: the

authors found pronounced static disorder in their X-ray powder diffraction data, leading to rms amplitudes of 50 pm for every atom; thus, the crystal structure is just an *average* over the true local minima. This lead Kroll, Riedel and Hoffmann to suggest two structural models in search of the actual structure, similar to α- and β-cristobalite [39]. We have performed additional phonon calculations on these suggested structures (shown in the supplementary information) and found imaginary frequencies as well, attributable to the same kind of vibrations as present in the experimental averaged cell. We therefore conclude that the exact nature of the true structure of SiC_2N_4 is a problem that remains to be solved and stick to the average structure for the purpose of this study. Regardless of how SiC_2N_4 exactly looks like, the vibrations of the NCN-units are an experimentally substantiated fact, as evident from the negative thermal expansion.

Since the proposed TY-carbodiimide is constructed in a similar way (Fig. 7, right top) as the experimental SiC_2N_4 structure, it is no surprise that the NCN-units show similar oscillations leading to imaginary modes in roughly the same frequency window. Thus, it is quite likely that C_3N_2 is actually kinetically stable, just like SiC_2N_4.

Given a successful synthesis, will TY-carbodiimide inherit the property portfolio that sparked the interest in TY-carbon in the first place? Analyzing its electron structure in terms of its symmetry inequivalent bonds, the answer has to be definitely yes, since the bonding pattern is reproduced with remarkable similarity (Fig. 8).

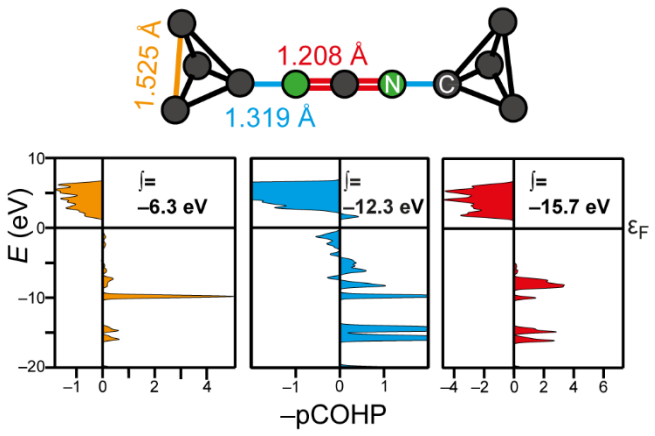

Figure 8: Projected COHPs for the three symmetry inequivalent bonds in carbodiimide-modified TY-carbon.

The COHP of the intra-tetrahedral bond looks very similar to its counterpart in TY-carbon: exclusively comprised of bonding levels and with molecule-like flat bands. Both bonds feature a big peak at –10 eV. Although the bond is of virtually the same length (Δd = 0.014 Å), it is weaker by 0.5 eV compared to TY-carbon. For all six bonds inside a tetrahedral unit, this totals to a difference of 3 eV. This is partially compensated by the other bonds: the connecting bond between the tetrahedron and the NCN-unit is stronger by 1.3 eV and shows the antibonding fingerprint typical for the tetrahedral topology. The triple bond that connects the two spacer atoms in TY-carbon is replaced in TY-carbodiimide by the two short double bonds in the NCN-unit. Each bond is individually stronger by 0.2 eV than the triple bond in TY-carbon. Still, TY-carbon is estimated to be more stable than TY-carbodiimide by a small amount of 14.8 kJ/mol in the total energy. For completeness, we also considered an interpenetrating version of TY-carbodiimide (TY-II-carbodiimide), which shows no stability improvement over the non-penetrating version (ΔE ~ 0.6 kJ/mol). This is due to the very large distances between the penetrating structure parts exceeding 5.6 Å. Detailed information is to be found in the supplement.

4. Summary

In conclusion, vital information about the bonding nature of proposed novel carbon allotropes which display tetrahedral symmetry is added to the knowledge about these promising candidates for future carbon-only functional materials. A characteristic bonding signature that carries along with the tetrahedral symmetry was discovered, which is comprised of an antibonding region of filled levels in the pCOHP, occupying an energy window ranging from –2 to –5 eV. This antibonding feature is created by the system's strain introduced by bonding

angles significantly deviating from the ideal of the according parent allotrope, as exemplified for the case of T-carbon and diamond. This strain leads to less efficient s- and p-level mixing than usually seen in carbon allotropes and makes the p-orbitals of different atoms slightly repel each other. Nevertheless, the bonds including the antibonding fingerprint are also the strongest ones in T-carbon, contributing mostly to the stability of the solid. TY-carbon's lower total energy is due to its possibility to push electron density further away from the strained tetrahedra into the C≡C triple bonds between the T-units. While there has been no feasible synthesis route to TY-carbon been suggested so far, we proposed a pathway to a similar compound dubbed TY-carbodiimide, that exhibits similar bonding properties and might be obtained from fully chlorinated C-tetrahedra and cyanamide. As gaseous hydrochloric acid is produced as a by-product, this will aid the endothermic reaction to fully go to the side of the products.

The bonding angles in T-graphene deviate the least from its parent allotrope graphene (90° instead of 120°). Even though the antibonding fingerprint shows up in the pCOHPs, too, the bonds are less strained and thus lead to the lowest total energy of the tetrasymmetrical allotropes.

Acknowledgements

We thank Volker L. Deringer for insightful discussions that helped to improve this work. The authors are grateful for support by the Russian Government (Grant 14.B25.31.0005) and by the Volkswagen Foundation (Deductive Quantum Molecular Mechanics of Carbon Allotropes).

References

[1] H. W. Kroto, J. R. Heath, S. C. O'Brien, R. F. Curl and R. E. Smalley, C_{60}: Buckminsterfullerene, Nature 318 (1985) 162–163.

[2] E. Osawa, Kagaku 25 (1970) 854. Non-japanese speakers are referred to: E. Osawa, H. W. Kroto, P.W. Fowler, E. Wassermann, The Evolution of the Football Structure for the C_{60} Molecule: A Retrospective [and Discussion], Phil. Trans. R. Soc. Lond. A 343 (1993) 1–8.

[3] http://sacada.sctms.ru; R. Hoffmann, A. A. Kabanov, A. A. Golov, D. M. Proserpio, Homo Citans and Carbon Allotropes: For an Ethics of Citation, Angew. Chem. Int. Ed. 55 (2016) 10962–10976.

[4] G. Dennler, M. C. Scharber, C. J. Brabec, Polymer-Fullerene Bulk-Heterojunction Solar Cells, Adv. Mater. 21 (2009) 1323–1338.

[5] S. Iijima, Helical microtubules of graphitic carbon, Nature 354 (1991) 56–58.

[6] K. S. Novoselov, A. K. Geim, S. V. Morozov, D. Jiang, Y. Zhang, S. V. Dubonos, et al., Electric field effect in atomically thin carbon films, Science 306 (2004) 666–669.

[7] A. Hirsch, The era of carbon allotropes, Nat. Mater. 9 (2010) 868–871.

[8] X.-L. Sheng, Q.-B. Yan, F. Ye, Q.-R. Zheng, G. Sung, T-Carbon: A Novel Carbon Allotrope, Phys. Rev. Lett. 106 (2011) 155703-1–155703-4.

[9] J. Y. Jo, B. G. Kim, Carbon allotropes with triple bond predicted by first-principle calculation: Triple bond modified diamond and T-carbon, Phys. Rev. B 86 (2012) 075151-1–075151-5.

[10] Y. Liu, G. Wang, Q. Huang, L. Guo, X. Chen, Structural and Electronic Properties of T Graphene: A Two-Dimensional Carbon Allotrope with Tetrarings, Phys. Rev. Lett. 108 (2012) 225505-1–225505-5.

[11] M. O'Keeffe, M. A. Peskov, S. J. Ramsden, O. M. Yaghi, The Reticular Chemistry Structure Resource(RCSR) Database of, and Symbols for, Crystal Nets, Acc. Chem. Res. 41 (2008), 1782–1789

[12] A.T. Balaban , C. C. Rentia, E. Ciupitu, Chemical Graphs. 6. Estimation of Relative Stability of Several Planar and Tridimensional Lattices for Elementary Carbon, Rev. Roum. Chim. 13 (1968) 231–247; Corrigendum: A. T. Balaban, C. C. Rentia, E. Ciupitu, Rev. Roum. Chim. 13 (1968) 1233.

[13] A. N. Enyashin, A. L. Ivanovskii, Graphene allotropes, Phys. Status Solidi B 248 (2011), 1879–1883.

[14] R. Dronskowski, P. E. Blöchl, Crystal Orbital Hamilton Populations (COHP). Energy-Resolved Visualization of Chemical Bonding in Solids based on Density-Functional Calculations, J. Phys. Chem. 97 (1993) 8617–8624.

[15] M. Esser, V. L. Deringer, R. Dronskowski, Orbital mixing in solids as a descriptor for materials mapping, Solid State Commun. 203 (2015) 31–34.

[16] J. P. Perdew, K. Burke, M. Ernzerhof, Generalized Gradient Approximation Made Simple, Phys. Rev. Lett. 77 (1996) 3865–3868.

[17] P. E. Blöchl, Projector augmented-wave method, Phys. Rev. B 50 (1994) 17953–17979.

[18] G. Kresse, J. Furthmüller, Efficient iterative schemes for ab initio total-energy calculations using a plane-wave basis set, Phys. Rev. B 54 (1996) 11169–11186.

[19] G. Kresse, J. Furthmüller, Efficiency of ab-initio total energy calculations for metals and semiconductors using a plane-wave basis set, Comput. Mater. Sci. 6 (1996) 15–50.

[20] G. Kresse, D. Joubert, From ultrasoft pseudopotentials to the projector augmented-wave method, Phys. Rev. B 59 (1999) 1758–1775.

[21] H. J. Monkhorst, J. D. Pack, Special points for Brillouin-zone integrations, Phys. Rev. B 13 (1976), 5188–5192.

[22] A. Togo, F. Oba, I. Tanaka, First-principles calculations of the ferroelastic transition between rutile-type and $CaCl_2$-type SiO_2 at high pressures, Phys. Rev. B 78 (2008) 134106-1–134106-9.

[23] V. L. Deringer, A. L. Tchougréeff, R. Dronskowski, Crystal Orbital Hamilton Population (COHP) Analysis as Projected from Plane-Wave Basis Sets, J. Phys. Chem. A 115 (2011) 5461–5466.

[24] S. Maintz, V. L. Deringer, A. L. Tchougréeff, R. Dronskowski, Analytic Projection from Plane-Wave and PAW Wavefunctions and Application to Chemical-Bonding Analysis in Solids, J. Comput. Chem. 34 (2013) 2557–2567.

[25] S. Maintz, V. L. Deringer, A. L. Tchougréeff, R. Dronskowski, LOBSTER: A tool to extract chemical bonding from plane-wave based DFT, J. Comput. Chem. 37 (2016) 1030–1035.

[26] V. L. Deringer, W. Zhang, M. Lumeij, S. Maintz, M. Wuttig, R. Mazzarello, R. Dronskowski, Bonding nature of local structural motifs in amorphous GeTe, Angew. Chem. Int. Ed. 53 (2014) 10817–10820.

[27] S. Yuk, A. Asthagiri, A first-principles study of Pt thin films on SrTiO3(100): Support effects on CO adsorption, J. Chem. Phys. 142 (2015) 124704-1–124704-10.

[28] V. L. Deringer, R. Dronskowski, Pauling's third rule beyond the bulk: chemical bonding at quartz-type GeO_2 surfaces, Chem. Sci. 5 (2014) 894–903.

[29] X. M. Zhang, A. Z. Wang, M. W. Zhao, Spin-gapless semiconducting graphitic carbon nitrides: A theoretical design from first principles, Carbon 84 (2015) 1–8.

[30] S. Maintz, M. Esser, R. Dronskowski, Efficient rotation of local basis functions using real spherical harmonics, Acta Phys. Pol. 47 (2016) 1165–1175.

[31] D. Li, F. Tian, D. Duan, Z. Zhao, Y. Liu, B. Chu, X. Sha, L. Wang, B. Liu, T. Cui, Modulated T carbon-like carbon allotropes: an ab initio study, RSC Adv. 4 (2014) 17364–17369.

[32] F. Tian, J. Wang, Z. He, Y. Ma, L. Wang, T. Cui, C. Chen, B. Liu, G. Zou, Superhard semiconducting C_3N_2 compounds predicted via first-principles calculations, Phy. Rev. B 78

(2008) 235431-1–235431-6.

[33] G. Maier, S. Pfriem, U. Schäfer, R. Matusch, Tetra-*tert*-butylcyclopentadienone, Angew. Chem. Int. Ed. Engl. 17 (1978) 520–521.

[34] R. Riedel, E. Kroke, A. Greiner, A. O. Gabriel, L. Ruwisch, J. Nicolich, Inorganic Solid-State Chemistry with Main Group Element Carbodiimides, Chem. Mater. 10 (1998) 2964–2979.

[35] X. Liu, M. Krott, M. Müller, C. Hu, H. Lueken, R. Dronskowski, Synthesis, crystal structure, and properties of MnNCN, the first carbodiimide of a magnetic transition metal, Inorg. Chem. 44 (2005) 3001–3003.

[36] X. Tang, H. Xiang, X. Liu, M. Speldrich, R. Dronskowski, A ferromagnetic carbodiimide: $Cr_2(NCN)_3$, Angew. Chem. Int. Ed. 49 (2010) 4738–4742.

[37] R. Riedel, A. Greiner, G. Miehe, W. Dressler, H. Fuess, J. Bill, F. Aldinger, The First Crystalline Solids in the Ternary Si-C-N System, Ang. Chem. Int. Ed. Engl. 36 (1997) 603–606.

[38] P. Kroll, M. Andrande, X. Yan, E. Ionescu, G. Miehe, R. Riedel, Isotropic Negative Thermal Expansion in β-$Si(NCN)_2$ and Its Origin, J. Phys. Chem. C 116 (2012) 526–531.

[39] P. Kroll, R. Riedel, R. Hoffmann, Silylated carbodiimides in molecular and extended structures, Phys. Rev. B 60 (1999) 3126–3139.